

ChemComm

Accepted Manuscript



This is an *Accepted Manuscript*, which has been through the Royal Society of Chemistry peer review process and has been accepted for publication.

Accepted Manuscripts are published online shortly after acceptance, before technical editing, formatting and proof reading. Using this free service, authors can make their results available to the community, in citable form, before we publish the edited article. We will replace this *Accepted Manuscript* with the edited and formatted *Advance Article* as soon as it is available.

You can find more information about *Accepted Manuscripts* in the [Information for Authors](#).

Please note that technical editing may introduce minor changes to the text and/or graphics, which may alter content. The journal's standard [Terms & Conditions](#) and the [Ethical guidelines](#) still apply. In no event shall the Royal Society of Chemistry be held responsible for any errors or omissions in this *Accepted Manuscript* or any consequences arising from the use of any information it contains.

Endohedrally Functionalised Porous Organic Cages

Alexandre Burgun^a, Peter Valente^a, Jack D. Evans^{a,b}, David M. Huang^a, Christopher J. Sumbly^{a*} and Christian J. Doonan^{a*}

Received 00th January 20xx,
Accepted 00th January 20xx

DOI: 10.1039/x0xx00000x

www.rsc.org/

The synthesis and characterisation of two novel, functionalised porous organic cages are presented. We demonstrate that a step-wise approach to the synthesis of these robust C-C bonded cages allows for the introduction of a controlled number of endohedral pyridine functional groups. In addition, kinetic processing is used to access permanently porous morphologies.

Shape-persistent organic cages are of growing interest to chemists as ‘building blocks’ for novel porous molecular solids.¹ Indeed, recent work has demonstrated that cage-based materials can exhibit unique adsorption properties due to their discrete nature and bespoke pore structures. For example, Cooper and co-workers have shown exceptional selectivity for niche separations such as those of noble gases and sulfur hexafluoride.² In addition, cage molecules are chemically versatile and can be processed into mixed-matrix membranes³ and thin films,⁴ covalently linked into porous polymers⁵ and judiciously functionalised to realise a permanently porous liquid phase.⁶

Given that organic cages offer a rich source of fundamental research and promising applications in materials science, the design and characterisation of new examples is of significant importance. Organic cages are typically synthesised using dynamic covalent chemistry and salient examples include imine,⁷ boronate ester condensations⁸ and alkyne metathesis.⁹ This approach has considerable appeal as cage molecules can be generated in high yields via a single-step synthesis. However, this strategy does not facilitate the construction of cages composed of multiple functional groups at precisely defined positions. In addition, the structural topology of the products cannot be predicted, with certainty, a priori.¹⁰ Here we report the synthesis, structures and porosity of two novel organic cage molecules via step-wise

carbon-carbon coupling reactions, C1-N2 and C1-N6 (Fig. 1). These materials illustrate the potential of this design concept for yielding molecular solids of functionally ‘programmed pores’.¹¹ Furthermore, cages constructed from carbon-carbon bonds are both chemically and thermodynamically robust¹² allowing for the chemistry of this class of materials to be significantly expanded.

Our initial attempt to synthesise cage C1-N6 was carried out using the intermolecular coupling method (Scheme S12) previously described in the literature.¹² This afforded cage C1-N6 in very low yields (4%). Therefore, we designed a new multi-step synthetic route, inspired by the procedures to prepare butadiyne-bridge square macrocycles¹³ and other cages of three-fold symmetry,¹⁴ where the ultimate reaction is a high-yielding intramolecular coupling. Accordingly, cages C1-N2 and C1-N6 were synthesised via the step-wise coupling

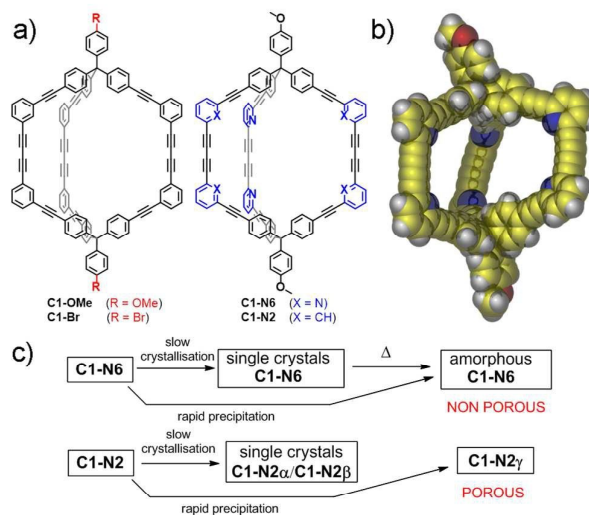
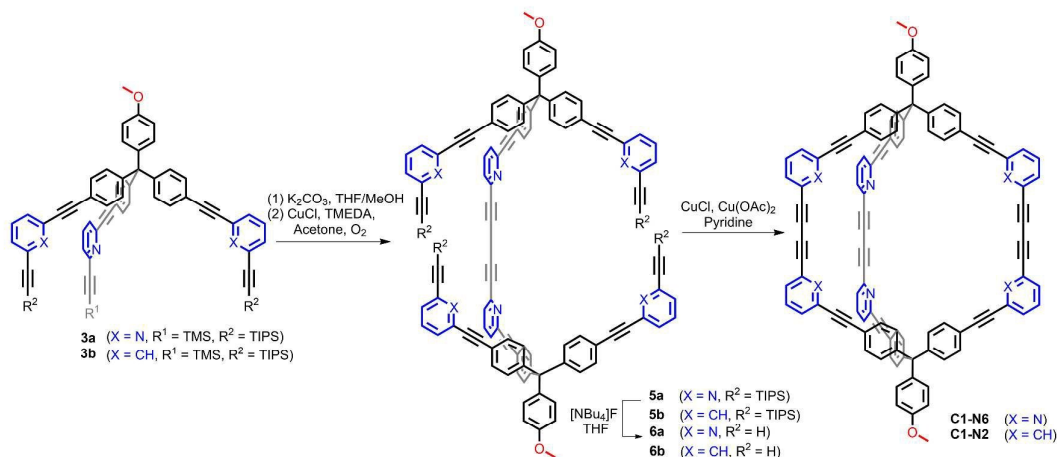


Fig. 1. (a) The structures of the previously reported all carbon-bonded cages C1-OMe and C1-Br and the new contributions C1-N2 and C1-N6 prepared in this work. (b) A space-filling representation of C1-N6 (C, yellow; N, blue; O, red; H, white). (c) A summary of the single crystal and rapidly precipitated phases reported in the manuscript.

^a Department of Chemistry and the Centre for Advanced Nanomaterials, The University of Adelaide, Adelaide, SA 5005, Australia

^b Present address: Chimie ParisTech, PSL Research University, CNRS, Institut de Recherche de Chimie Paris, 75005 Paris, France

Electronic Supplementary Information (ESI) available: synthetic details for C1-N2 and C1-N6, NMR spectra, additional characterisation. See DOI: 10.1039/x0xx00000x



Scheme 1. The step-wise 'clipped' synthesis of C1-N2 and C1-N6.

procedure delineated in Scheme 1 (see Scheme S11 for full details). A key step to this approach involves the mono-substitution of the tripodal building block 4-[tris(4-iodophenyl)methyl]methoxybenzene (**1**), via a Sonogashira coupling with a trimethylsilyl protected pyridine moiety to afford compound **2**. A similar synthetic approach was employed using triisopropylsilyl protected phenyl (for C1-N2) or pyridine units (for C1-N6) to functionalise both available positions in **2**. Compound **3** was then selectively deprotected at the trimethylsilyl position and dimerised by a Hay coupling reaction to give the triisopropylsilyl protected dimer **5**. Silyl deprotection of compound **5** was achieved with tetrabutylammonium fluoride to yield the deprotected dimer **6**. Isolated yields for each of the synthetic steps described above were generally good to excellent (between 60 to 99%). The final intramolecular carbon-carbon homo-coupling reaction was completed using the standard synthetic method previously described¹² for the formation of cage and macrocycle compounds, such as C1-OMe and C1-Br. Under high dilution conditions in pyridine, and with the presence of a large excess of copper catalysts, the reaction proceeds to favour the formation of kinetic products C1-N2 or C1-N6. After purification, cages C1-N2 and C1-N6 were obtained in good yields (53% and 52% yield, respectively) compared with the intermolecular homo-coupling approach, for which final step yields are about 20%.

The formation of C1-N2 and C1-N6 was confirmed by ¹H and ¹³C NMR, Infrared spectroscopy (IR), and high resolution mass spectrometry (HRMS). The most noteworthy features of the ¹H NMR and IR spectra are the disappearance of the peaks attributable to the alkyne protons of **6**. For example, the IR of C1-N2 and C1-N6 are devoid of the C_{alkyne}-H stretch found in **6a** and **6b** at 3289 cm⁻¹; however, the C=C stretches at 2200–2220 cm⁻¹ are retained. Additionally, the HRMS of C1-N2 and C1-N6 afford [M + H]⁺ parent ions at m/z 1441.47 (C1-N2) and 1445.45 (C1-N6). Cages C1-N2 and C1-N6 are soluble in common organic solvents such as acetone, tetrahydrofuran,

benzene and halogenated solvents but are poorly soluble or insoluble in alcohols, water, alkanes and acetonitrile.

Single crystals of C1-N2 and C1-N6 suitable for X-ray crystallography were grown by slow diffusion of petroleum spirits into a benzene solution of C1-N2, and hexane into a toluene solution of C1-N6. A single crystalline polymorph of C1-N6 was isolated in this work (yellow rods, triclinic, *P*-1). However, C1-N2 was found to crystallise as a mixture of two distinct forms: C1-N2 α , as colourless rod-shaped crystals (tetragonal, *I*₄₁/*acd*), and C1-N2 β as colourless plate-like crystals (orthorhombic, *Pbcn*). Due to the rigid nature of the molecular backbone of the cages, the vertical and horizontal outer dimensions of both C1-N6 and C1-N2 are broadly similar (*ca.* 3.0 by 1.5 nm) to previously reported examples^{12, 15} but herein these enclose an internal cavity comprising six or two pyridine substituents, respectively. In the solid-state, the pyridine substituents lead to a more distorted cage than observed for the phenyl shouldered cages; the angles about the cage shoulder (alkynyl-pyridine-alkyne centroid angles) range from 111.2 to 117.2° for C1-N6 compared with the equivalent angle range for C1-OMe (117.3–120.4°). These distortions, coupled with a more twisted arrangement, produce a C1-N6 cage with more squat dimensions, specifically a quaternary C–C separation of 15.5 Å compared with 18.0, 16.8 and 17.9 Å in C1-OMe, C1-N2 α and C1-N2 β , respectively. The extensive distortion for the C1-N6 cage results in a crystalline packing that has not been observed for either of the parent phenyl cages C1-OMe and C1-Br. In contrast, the β -form of C1-N2 is isomorphous with cage C1-OMe (*Pbcn*) and crystallises with four molecules in the unit cell. Similarly, the tetragonal α -phase packs identically to C1-Br. Examination of the densities of the three crystal structures (in the absence of solvates; SQUEEZE routine of Platon¹⁶ applied) reveals the α -phase of C1-N2 is the least dense form (0.62 g.cm⁻³) while the β phase possesses the most dense structure (0.83 g.cm⁻³). Cage C1-N6 has an intermediate density packing (0.72 g.cm⁻³). Close examination of all crystal structures reveals that the primary inter-cage interactions in the crystal packing are van

der Waals interactions and edge-to-face π -interactions involving both phenyl/pyridyl and alkyne moieties (Fig. 2). The simulated N_2 probe accessible pore surfaces shows that C1-N2 α and C1-N2 β possess notably different pore network structures; C1-N2 α possesses a connected 3D pore network, while C1-N2 β has 1D channels comprised of adjacent cages linked by ~ 4.1 Å windows, as observed for C1-OMe. In the case of C1-N6, simulation of the N_2 probe accessible pore surface reveals a pore network that extends only in the a and b axis directions with limiting pore diameters of ~ 5.1 Å.

We examined the bulk crystallinity of C1-N2 and C1-N6 by Powder X-ray Diffraction (PXRD) methods. Notably the behaviour of the two cages in the solid-state depended on processing methods. PXRD performed on samples comprising C1-N6 single crystals supported phase purity (Figure S17); however, we were unable to obtain microcrystalline samples via solvent evaporation (CH_2Cl_2) or by grinding dried crystals. In contrast, rapid precipitation of C1-N2 (from CH_2Cl_2 /methanol) gave rise to a new crystalline polymorph C1-N2 γ (Figure S16). Notably, C1-N2 γ is identical to the rapidly crystallised phase obtained for C1-OMe.¹² Additionally, experimental powder diffraction patterns of polymorphs C1-N2 α and C1-N2 β (Figure S15) were obtained by manually separating a small amount of rod and plate-like crystals from the bulk sample.

The permanent porosity of C1-N2 and C1-N6 was investigated by 77K N_2 gas adsorption experiments. As noted,

we were unable to obtain crystalline samples of C1-N6 for adsorption analysis. Rapid precipitation of C1-N6 led to an amorphous solid whilst desolvation (under vacuum at room temperature or at 80°C) of a single crystal sample resulted in a change from a crystalline to an amorphous phase. Although porosity in the amorphous phase has been demonstrated for organic cages as a result of 'frustrated' solid-state packing,¹⁷ cage C1-N6 was found to be non-porous to N_2 . We then performed a 77K N_2 gas adsorption isotherm on the phase pure polymorph C1-N2 γ (C1-N2 α and C1-N2 β were only isolated on a large scale as a mixed phase). The resultant isotherm (Figure S18) is best described as Type I; however, a noticeable hysteresis is observed on desorption over a range of equilibration times. Such hysteretic behaviour may arise from an amorphous phase not detected by PXRD methods. Thus, we employed scanning electron microscopy (SEM) to inspect the morphology of C1-N2 γ . Figure S19 indicates that polymorph C1-N2 γ uniformly consists of thin plate-like crystals which are formed rapidly upon precipitation, with crystals size in the range 1 and 10 μm . Indeed, the crystal morphology was analogous to that observed for C1-OMe.¹²

Previously we reported the synthesis and characterisation of an analogous cage (C1-OMe) via a three-fold homo-coupling macrocyclisation reaction (20% yield). However, in contrast to C1-OMe this approach afforded significantly diminished yields for C1-N6 of ca. 4% (Scheme S12). We did not attempt to synthesise C1-N2 using the intermolecular homo-coupling employed for C1-OMe as, in addition to potentially low yields, such conditions would be expected to form a statistical mixture of isomers. Thus, we turned our efforts to understanding why the intermolecular coupling reaction to form C1-N6 engendered reproducibly low yields. The salient difference between the cages is the presence of pyridine groups in the molecular framework of C1-N6. Pyridine moieties are known to influence packing arrangements in supramolecular systems as a result of dipole-dipole interactions.¹⁸ To this end we employed density functional theory (DFT) to ascertain if the significantly lower yields could be accounted for by electronic arguments. Molecular structures and energies of C1-OMe and C1-N6 cages and half-cage precursors were computed by DFT using the Gaussian 09 (Revision D.01) software package.¹⁹ Half-cage molecules were obtained by breaking the full cage in half and terminating the ethynyl groups with hydrogens. The DFT calculations show that the maximum electrostatic interaction energy and total interaction energy between two half-cages brought into sufficiently close proximity to permit homo-coupling were negligible both *in vacuo* and in implicit pyridine solvent for both C1-N6 and C1-OMe, with the interactions somewhat larger for the C1-N6 half-cages due to their considerably larger dipole moments (see Supporting Information for full description of calculations). Thus, DFT analysis infers that unfavourable electrostatic interactions between half-cages can be excluded as an explanation for the relatively low yields recorded for C1-N6. An alternative explanation involves the bond angle of the corner unit: C-C_{ph}-C vs C-N_{py}-C. As described above, there is a significant difference in the corner unit angles

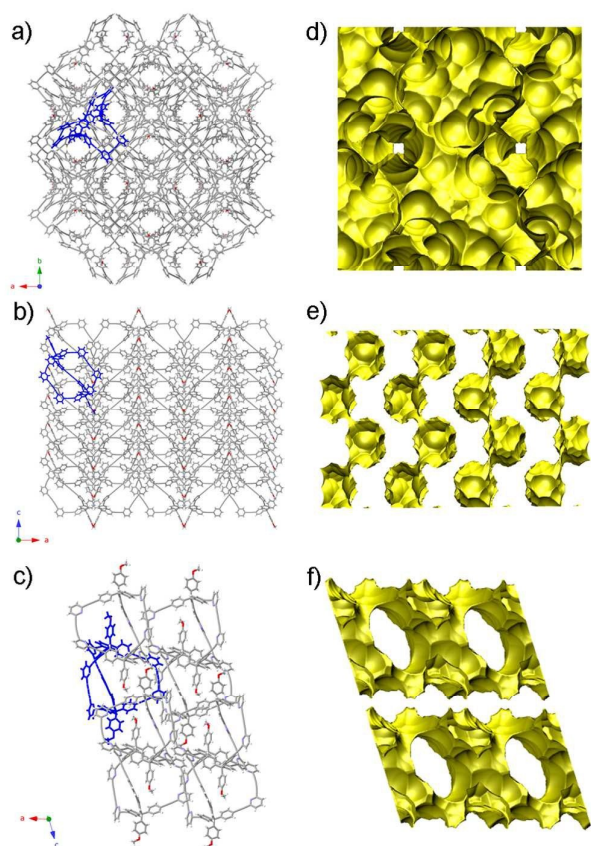


Fig. 2. Rod and stick representations of the structures of a) C1-N2 α down the c axis, b) C1-N2 β down the b axis, and c) C1-N6 down the b axis. Corresponding views of the probe accessible surface area (N_2 probe) in the crystal structures d) C1-N2 α , e) C1-N2 β and f) C1-N6.

between cages C1-OME and C1-N6, yielding a more distorted cage molecule in the case of C1-N6 in the solid-state (although in vacuo/implicit pyridine optimised structures suggest the cage distortion is limited, Fig. S110 and S111). Accordingly, given that the carbon-carbon coupling reactions used to construct the cages are irreversible, it can be proposed that a potentially distorted C1-N6 precursor will lead to slower reaction rates and to the formation of polymeric/oligomeric species by-products.

Conclusions

We have synthesised two new cage molecules C1-N2 and C1-N6 via a stepwise approach that leads to precise control of pore functionality. Furthermore, C1-N2 can be isolated as a porous solid by rapid precipitation from solution. We note that analogous chemistry is not observed for C1-N6 suggesting that subtle structural modifications can have a dramatic effect on crystal packing and the resultant performance characteristics of the material. The synthetic strategy outlined in this work is of significant fundamental interest to the field as it provides broad scope for generating novel unsymmetrical porous cage molecules with precisely functionalised pore chemistry. We anticipate that such control over the internal functionality of the cages will facilitate the precise tuning of their performance characteristics. For example, the pyridine moieties described in this work could support post-synthetic metalation chemistry; a strategy that has been successfully employed to tailor the properties of Metal-organic Frameworks.²⁰

Notes and references

This research is supported by the Australian Research Council and the Science and Industry Endowment Fund (SIEF). Aspects of this research were undertaken on the MX beamlines at the Australian Synchrotron, Victoria, Australia and with the assistance of resources provided at the NCI National Facility systems through the National Computational Merit Allocation Scheme supported by the Australian Government. We would like to thank Ms Georgina Sylvia for experimental assistance and Mr Patrick Capon for recording the SEM images.

- G. Zhang and M. Mastalerz, *Chem. Soc. Rev.*, 2014, **43**, 1934; J. D. Evans, C. J. Sumby and C. J. Doonan, *Chem Lett.*, 2015, **44**, 582; A. G. Slater and A. I. Cooper, *Science*, 2015, **348**, 988; Y. Jin, Q. Wang, P. Taynton and W. Zhang, *Acc. Chem. Res.*, 2014, **47**, 1575.
- T. Hasell, M. Miklitz, A. Stephenson, M. A. Little, S. Y. Chong, R. Clowes, L. Chen, D. Holden, G. A. Tribello, K. E. Jelfs and A. I. Cooper, *J. Am. Chem. Soc.*, 2016, **138**, 1653; L. Chen, P. S. Reiss, S. Y. Chong, D. Holden, K. E. Jelfs, T. Hasell, M. A. Little, A. Kewley, M. E. Briggs, A. Stephenson, K. M. Thomas, J. A. Armstrong, J. Bell, J. Busto, R. Noel, J. Liu, D. M. Strachan, P. K. Thallapally and A. I. Cooper, *Nat. Mater.*, 2014, **13**, 954.
- A. F. Bushell, P. M. Budd, M. P. Atfield, J. T. A. Jones, T. Hasell, A. I. Cooper, P. Bernardo, F. Bazzarelli, G. Clarizia and J. C. Jansen, *Angew. Chem. Int. Ed.*, 2013, **52**, 1253; T. Mitra, R. S. Bhavsar, D. J. Adams, P. M. Budd and A. I. Cooper, *Chem. Commun.*, 2016, **52**, 5581.
- Q. Song, S. Jiang, T. Hasell, M. Liu, S. Sun, A. K. Cheetham, E. Sivaniah and A. I. Cooper, *Adv. Mater.*, 2016, **28**, 2629.
- O. Buyukcakir, Y. Seo and A. Coskun, *Chem. Mater.*, 2015, **27**, 4149; Y. Jin, B. A. Voss, R. McCaffrey, C. T. Baggett, R. D. Noble and W. Zhang, *Chem. Sci.*, 2012, **3**, 874.
- N. Giri, M. G. Del Pópolo, G. Melaugh, R. L. Greenaway, K. Rätzke, T. Koschine, L. Pison, M. F. Costa Gomes, A. I. Cooper and S. L. James, *Nature*, 2015, **527**, 216.
- T. Tozawa, J. T. A. Jones, S. I. Swamy, S. Jiang, D. J. Adams, S. Shakespeare, R. Clowes, D. Bradshaw, T. Hasell, S. Y. Chong, C. Tang, S. Thompson, J. Parker, A. Trewin, J. Bacsa, A. M. Z. Slawin, A. Steiner and A. I. Cooper, *Nat. Mater.*, 2009, **8**, 973.
- G. Zhang, O. Presly, F. White, I. M. Oppel and M. Mastalerz, *Angew. Chem. Int. Ed.*, 2014, **53**, 1516.
- C. Zhang, Q. Wang, H. Long and W. Zhang, *J. Am. Chem. Soc.*, 2011, **133**, 20995; S. Lee, A. Yang, T. P. Moneyppennyll and J. S. Moore, *J. Am. Chem. Soc.*, 2016, **138**, 2182.
- Q. Wang, C. Yu, C. Zhang, H. Long, S. Azarnoush, Y. Jin and W. Zhang, *Chem. Sci.*, 2016, **7**, 3370.
- L. Liu, K. Konstas, M. R. Hill and S. G. Telfer, *J. Am. Chem. Soc.*, 2013, **135**, 17731.
- A. Avellaneda, P. Valente, A. Burgun, J. D. Evans, A. W. Markwell-Heys, D. Rankine, D. J. Nielsen, M. R. Hill, C. J. Sumby and C. J. Doonan, *Angew. Chem. Int. Ed.*, 2013, **52**, 3746.
- M. Sonoda, Y. Yamaguchi, K. Tahara, K. Hirose and Y. Tobe, *Tetrahedron*, 2008, **64**, 11490; T. Zhao, Z. Liu, Y. Song, W. Xu, D. Zhang and D. Zhu, *J. Org. Chem.*, 2006, **71**, 7422.
- Z. Wu, S. Lee and J. S. Moore, *J. Am. Chem. Soc.*, 1992, **114**, 8730.
- M. Kitchin, K. Konstas, C. J. Sumby, M. L. Czyn, P. Valente, M. R. Hill, A. Polyzos and C. J. Doonan, *Chem. Commun.*, 2015, **51**, 14231.
- A. L. Spek, *Acta Crystallogr.*, 2009, **D65**, 148.
- S. Jiang, K. E. Jelfs, D. Holden, T. Hasell, S. Y. Chong, M. Haranczyk, A. Trewin and A. I. Cooper, *J. Am. Chem. Soc.*, 2013, **135**, 17818; T. Hasell, S. Y. Chong, K. E. Jelfs, D. J. Adams and A. I. Cooper, *J. Am. Chem. Soc.*, 2012, **134**, 588; J. D. Evans, D. M. Huang, M. R. Hill, C. J. Sumby, D. S. Sholl, A. W. Thornton and C. J. Doonan, *J. Phys. Chem. C*, 2015, **119**, 7746.
- B. K. Mishra and N. Sathyamurthy, *J. Phys. Chem. A*, 2005, **109**, 6.
- M. J. Frisch, G. W. Trucks, H. B. Schlegel, G. E. Scuseria, M. A. Robb, J. R. Cheeseman, G. Scalmani, V. Barone, B. Mennucci, G. A. Petersson, *et al.*, Gaussian 09 (Revision D.01), Gaussian, Inc., Wallingford CT, 2009.
- J. D. Evans, C. J. Sumby and C. J. Doonan, *Chem. Soc. Rev.* 2014, **43**, 5933.